International Journal of Greenhouse Gas Control 151 (2026) 104609

Contents lists available at ScienceDirect

International Journal of Greenhouse Gas Control

journal homepage: www.elsevier.com/locate/ijggc

Integrating baseline and 4D seismic to assess structural and stratigraphic influences on CO2 containment at Sleipner

Basil Onyekayahweh Nwafor [a,*], John P. Castagna [a], Robert Van Eykenhof [c], Marianne Rauch [b], David E. Bass [a]

[a] University of Houston, Houston, TX, USA
[b] Lumina Geophysical, Houston, TX, USA
[c] Lumina Geophysical, London, United Kingdom

ARTICLE INFO

Keywords:
CCUS
CO2
Sleipner
Synthetic Modelling
Monitoring
Time-lapse (4D) Seismic Data
Geologic storage

ABSTRACT

This study investigates the geologic controls governing CO_2 plume migration and trapping at the Sleipner storage site within the Utsira Formation, using a detailed conceptual model integrated with synthetic seismic simulation and attribute analysis. The model incorporates key stratigraphic features, stacked channel sands, thin shale drapes, and a critical 7–9 meter internal shale barrier, alongside structural elements such as polygonal faults. Synthetic seismic responses were generated for brine- and gas-saturated scenarios and validated against time-lapse (4D) seismic data acquired in 2010. Two conceptual migration scenarios were tested: one with CO_2 confined below the shale barrier, and another allowing upward migration into an overlying sand wedge. The second scenario successfully reproduced the observed "upward shift" anomaly, indicating a likely breach or bypass of the shale. Additionally, stratigraphic continuity attributes extracted from synthetic and real data suggest that channel terminations act as lateral plume boundaries. Quantitative metrics, including the plume coverage ratio and structural and stratigraphic margin capacity analyses, were developed to evaluate trapping mechanisms. Results show that only about 18% of the mapped stratigraphic boundary remains unfilled, demonstrating strong stratigraphic confinement, whereas approximately 85% of the structural margin area remains unutilized. These findings highlight the dominant influence of internal stratigraphy over structural features in governing CO_2 plume migration and provide valuable guidance for characterization and monitoring of future geologic carbon storage sites.

1. Introduction

Geological storage of carbon dioxide (CO_2) in deep saline aquifers is recognized as a key component of global efforts to reduce atmospheric greenhouse gas concentrations and mitigate climate change (Benson and Cole, 2008; IPCC, 2005). The Sleipner field in the Norwegian North Sea represents the world's first commercial-scale CO_2 storage project, with injection commencing in 1996 into the Utsira Formation, a large, unconsolidated saline sandstone aquifer located approximately 800–1000 m below the seabed (Arts et al., 2008; Chadwick et al., 2004).

The Sleipner CO_2 storage project has become a global benchmark for understanding CO_2 plume migration, trapping mechanisms, and reservoir dynamics, primarily due to its rich and continuous monitoring datasets, comprising repeated time-lapse (4D) seismic surveys and well log measurements. These datasets have shown that CO_2 does not migrate uniformly throughout the reservoir. Instead, it accumulates in a series of thin, laterally extensive layers, a behavior strongly influenced by internal stratigraphic heterogeneities and subtle structural features (Chadwick et al., 2010; Furre et al., 2017, 2024; Warchoł et al., 2025).

Despite the Utsira Sandstone being characterized by excellent reservoir properties, porosity ranging from 27 % to 42 % and permeability reaching up to 8 Darcy (Zweigel et al., 2004), initial plume migration was primarily vertical and highly confined. Lateral westward spreading occurred only recently (Furre et al., 2024). This vertical confinement is particularly noteworthy given the extensive and homogeneous nature of the Utsira Sand across the Sleipner area. Fig. 1 presents a gamma ray log illustrating the thick, clean, and laterally extensive Utsira Sandstone at the injection site. The log section is taken along a WSW–ENE axis by (Warchoł et al., 2025), which coincides with the direction in which the CO_2 plume shows lateral confinement. This

* Corresponding author at: University of Houston, Houston, Texas, USA.
E-mail address: bonwafor@uh.edu (B.O. Nwafor).

https://doi.org/10.1016/j.ijggc.2026.104609
Received 14 August 2025; Received in revised form 4 February 2026; Accepted 5 February 2026
Available online 14 February 2026

alignment suggests a possible stratigraphic or facies-related control on the plume's geometry.

Due to the inadequately resolved baseline survey and a limited grasp of the pre-injection geological characteristics of the reservoir, the interpretation of the storage reservoirs relied mostly on post-injection reflections. Seismic resolution refers to the ability of seismic data to distinguish between two closely spaced geological events in time or space. The baseline seismic volume (shown in Fig. 2) exhibits limited resolution and does not reveal any clear lateral barriers to plume migration within the injection interval. A clear indication of this limitation is the presence of vertical faults that remained unresolved in the baseline data but became distinctly visible in the higher-resolution monitor survey (Fig. 2). In the initial analysis of monitoring data, Chadwick et al. (2004), as well as Williams and Chadwick (2021), observed these vertical zones with diminished reflectivity and increased velocity pushdown situated approximately above the injection point (Fig. 2). This zone was construed as a vertical 'chimney,' assumed to be the primary pathway for the upward movement of CO_2 within the reservoir. As seen in Fig. 1, the intra-reservoir reflections within the injection interval became more prominent and thicker compared to the poorly resolved baseline seismic. The bright reflections mostly correspond to reflection doublets, which are two closely spaced seismic reflection events that appear as a pair of peaks and troughs (or two overlapping wavelets) on a seismic trace arising when two acoustic impedance contrasts (interfaces) are very close, causing their individual reflections to interfere with each other. This was interpreted by Arts (2004) as interference wavelets from thin layers of CO_2-saturated sand. This interference makes it impossible to correctly resolve the geology of the reservoir using post-injection seismic reflections. As there are no wells that penetrate the plume directly, the precise count of mudstone-sandstone layers interspersed within the plume envelope remains unknown.

Researchers have devoted significant attention to understanding the factors influencing CO_2 plume migration within the topmost layer of the Utsira Formation. A substantial body of published work has focused on characterizing and simulating plume behavior in this uppermost layer, given its importance in monitoring and containment assessment. The observed seismic response at the top of this layer is a composite effect of acoustic and elastic property variations within the layer. CO_2 migration within this interval is expected to behave like supercritical fluid movement, where buoyant CO_2 displaces denser brine and spreads laterally until constrained by structural or stratigraphic barriers. Plume modeling predicts that such migration should form an umbrella-shaped accumulation beneath the top seal. However, this geometry is not observed at Sleipner, prompting further investigation into the mechanisms controlling plume distribution and internal flow behavior. According to Chadwick et al. (2009), the topmost CO_2 accumulation is particularly critical for two key reasons: first, it enables the most accurate quantification of the plume's thickness and volume; and second, its vertical growth reflects the total upward flux of CO_2 through the reservoir and how this flux evolves over time.

Beyond quantification, the behavior of this layer is central to evaluating whether the CO_2 plume is likely to continue spreading or potentially breach the top of the Utsira Formation. However, despite extensive modeling and seismic monitoring, precise characterization of this topmost layer remains challenging. One unresolved question that continues to attract attention is whether the plume has reached the upper sand wedge, which is separated from the regional top Utsira surface by a relatively thin shale barrier approximately 7–9 m thick (Fig. 1). Determining whether this internal shale has been breached is pivotal to understanding the long-term integrity of the storage system, as well as predicting plume migration path at the top of the formation.

To understand the physical processes governing this layered accumulation, a geologic conceptual model was developed for the Utsira Formation, integrating seismic interpretation and petrophysical analysis. This model accounts for the influence of thin shale drapes, stacked channel systems, and polygonal faulting on plume behavior. Synthetic seismic modeling based on this framework provides crucial insights into the role of stratigraphic barriers and internal heterogeneities in CO_2 containment and plume geometry. The Utsira Formation has recently

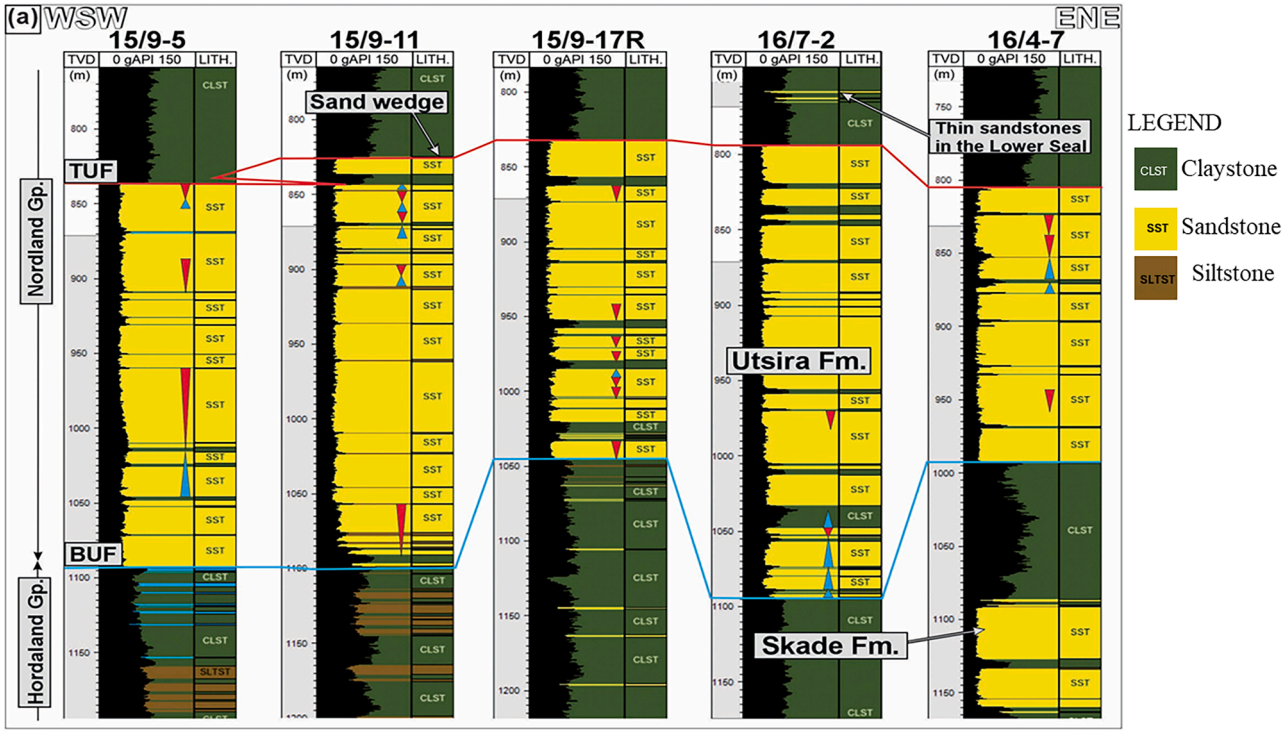

Fig. 1. WSW -ENE Gamma ray log section of the Utsira formation showing the Top (TUF and Base (BUF) of Utsira Formation, Sand wedge above the Utsira formation and the Skade Formation underlying the Utsira Formation (Warchoł et al., 2025).

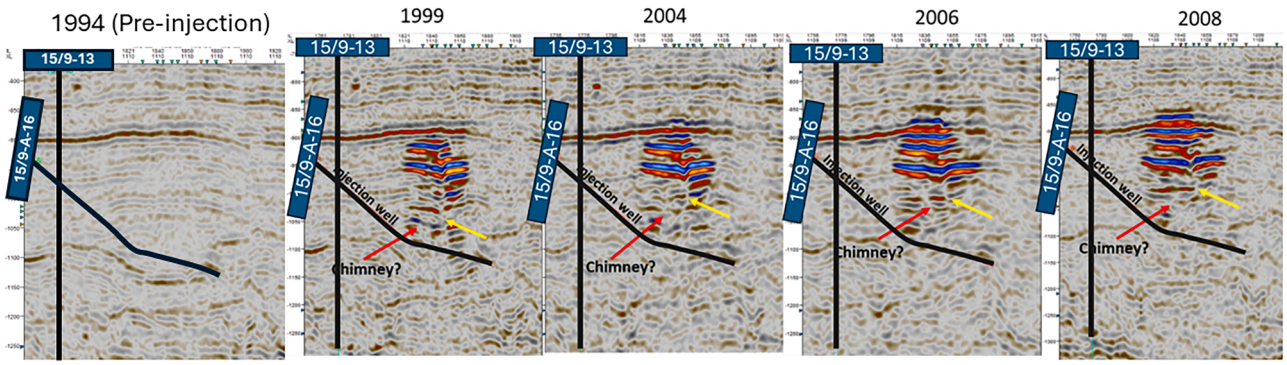

Fig. 2. Baseline and Time-lapse seismic sections through the injection site. The Baseline shows no obvious vertical fault for upward migration, but post-injection monitor suvery shows a vertical migration pathway above the injection point. The western vertical structure (red arrow) appears to have healed in the 2008 survey.

been reinterpreted as a medial to distal segment of a north to south oriented submarine fan system with extensive sediment bypass, forming incised valleys and channel complexes that serve as primary permeability modifiers (Nwafor et al., 2024; Warchoł et al., 2025). These erosional and depositional elements, identified in RGB attribute maps and stratigraphic continuity volumes, constrain plume migration laterally and vertically (Nwafor et al., 2024; Rauch et al., 2025, Warchoł et al., 2025).

One key question addressed in this study is whether the ~7–9-meter shale layer, which separates the main Utsira Sand from an overlying sand wedge, has been breached either before or during CO_2 injection. This has implications for vertical containment and the long-term integrity of the storage site and in predicting future migration paths as injection continues. Additionally, the study aims to quantify the relative influence of structural versus stratigraphic controls on CO_2 trapping by comparing the extent of the plume with seismic attributes indicative of geologic continuity and structural closure. Findings from apparent time thickness (ATT) and time-lapse RMS amplitude maps by Nwafor et al., 2025, indicate that localized intra-channel geobodies and channel margins, sometimes draped by discontinuous shale or bounded by steep incision surfaces, play a significant role in constraining plume extent (Furre et al., 2024; Warchoł et al., 2025).

By reconciling synthetic seismic responses with observed time-lapse data, and applying quantitative similarity metrics, this work enhances our understanding of the factors that govern CO_2 migration in saline aquifers. Ultimately, the findings contribute to improved predictive models for future CO_2 storage projects and underscore the critical role of high-resolution geologic characterization in site selection and long-term monitoring strategies.

2. Methodology

This study employed a comprehensive geophysical modeling and seismic analysis workflow to investigate the stratigraphic and structural controls on CO_2 plume migration within the Utsira Formation at the Sleipner Field. The depositional facies were assigned primarily based on facies interpretations from well logs and the published depositional model of the Utsira Formation from recent literatures. Warchoł et al. (2025) reported that the Utsira Formation represents an incised-valley to basin-floor fan system, characterized by a network of channelized sand bodies, fan lobes, and thin intraformational mud drapes. In their study, the incised valley was interpreted as a confined channel system eroded into underlying strata and subsequently filled with high-quality, well-sorted sands. The channels transition laterally and downdip into sheet-like fan lobes, while thin, discontinuous mudstone drapes and lobe-margin shales create internal heterogeneity and compartmentalization within the reservoir. These mud-rich layers are particularly important because they act as partial baffles to vertical CO_2 migration, while the sandy channel-fill facies provide the main pathways for lateral migration.

In constructing the model, these depositional facies were spatially distributed following the geometries interpreted from seismic reflection data, seismic attributes, and regional stratigraphic context. Channel-fill sands were assigned to the incised valley axis to represent high-porosity, high-permeability flow zones. Lobe sands were distributed distally as laterally continuous but thinner units. Thin shale or mud drape facies were inserted between the sand units and terminated at the channel edges. The overburden and underlying units were assigned average background properties based on the well log properties. This model (Fig. 3) captured the reservoir's complex heterogeneity, including stacked channel systems, and thin, laterally variable shale drapes. A critical feature of the model is the 7–9 m thick internal shale barrier that separates the main Utsira Sand from an overlying sand wedge. This shale unit, along with thinner 1–6 m shale layers interbedded throughout the reservoir, was included to simulate realistic vertical and lateral flow restrictions.

The geologic model was structured into multiple stratigraphic layers, reflecting both the depositional architecture and fault-induced compartmentalization. Vertical migration pathways were modeled as being influenced by sand body connectivity and fault presence, while lateral migration was subject to channel edge discontinuities and localized shale barriers. Previous studies have subdivided the plume reflections in the monitor survey into numbered layers. A recent publication by Furre et al. (2024) reports that the latest monitor survey, currently not publicly available, reveals a slight westward migration of the plume within Layers 6, 8, and 9. Particular attention was given to layers 6, 8, and 9, where plume geometry is thought to be influenced by gentle structural dips and subtle topographic closures.

A seismic model that is purposefully simplified, 2-D, and comparative, designed to test seismic consistency between conceptual leakage scenarios and the observed field data, rather than to represent a full elastic wave simulation was constructed. To construct the synthetic model, the model geometries were defined with offset axes expressed in meters and the depth axis in milliseconds, consistent with the coordinate framework of the actual seismic data and constrained to the analysis window of interest. A 2D grid was generated, and the stratigraphic layering and geobodies were delineated using polygonal outlines. Each layer polygon was then assigned rock properties derived from measured well-log parameters, including density ρ, compressional velocity, Vp and shear velocity Vs. As summarized in Table 1, the storage complex was subdivided into five main units: the overburden, sand wedge, thin shale (7–9 m), Utsira (main reservoir), and CO_2-saturated gas zone.

The acoustic impedance, AI for each layer was computed from the assigned rock properties using the standard relationship:

$$AI = \rho Vp$$

These impedance contrasts (shown in Fig. 4- left) were used to generate the reflectivity model (Fig. 4- right) using the Zoeppritz

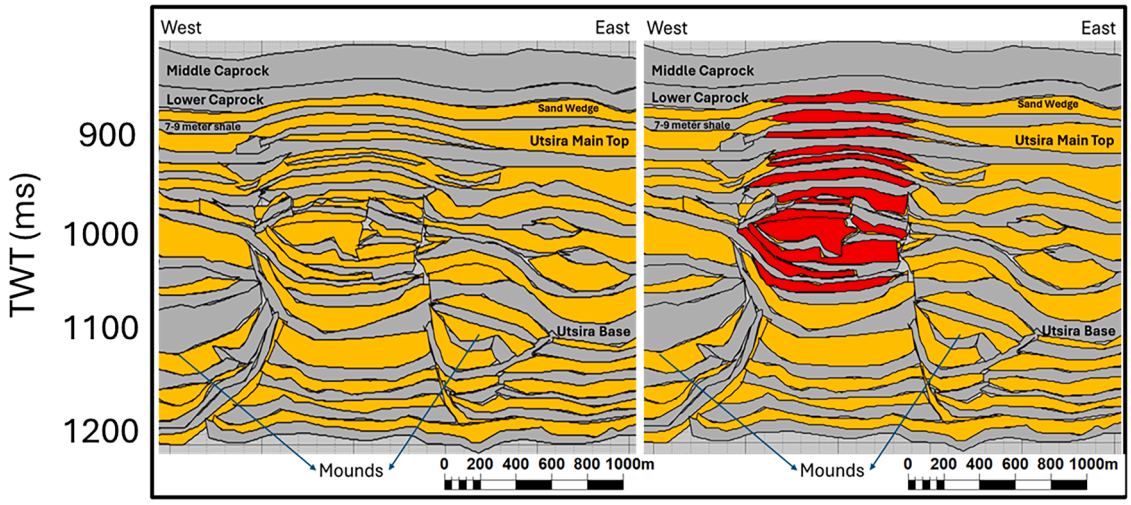

Fig. 3. *Geologic model of the Sleipner injection site showing CO_2 plume behavior.*
(a) Pre-injection model illustrating stacked channel systems, thin shale drapes, and a 7–9 m shale separating the sand wedge from the main Utsira Sand. Vertical migration is influenced by polygonal faults and partial sand connectivity. (b) Post-injection model showing plume trapping controlled by stratigraphy in lower layers and combined structural-stratigraphic effects in upper layers. The yellow filled layers are Utsira sand unit while the gray layers are the shale unit. The red filled layers are Sand Units filled by CO_2 Plumes. Vertical scale is 1:5.

Table 1
Rock property parameters for geological layers at the sleipner CO_2 injection site.

Layer Name	Vp (ft/s)	Vs (ft/s)	Rho (g/cc)	Poisson's
Overburden	7073	2634	2.02	0.4195
Sand wedge	13,409	8036	2.36	0.2198
Thin Shale (7–9 m)	6783	2647	2.06	0.4102
Utsira (main)	8061	3544	2.01	0.3802
Porous Gas Sand	6367	4365	1.937	0.0566

equations.

Subsequently, the reflection coefficients were convolved with a 30 Hz Ricker wavelet (Fig. 5) using convolutional model. The wavelet was chosen to match the dominant frequency of the baseline field seismic, ensuring spectral consistency between the synthetic and field dataset.

The resultant synthetic seismic model is shown in Fig. 6. Visually, the synthetic model and seismic data exhibit broadly similar overall patterns when noise effects are disregarded, indicating that the modeled stratigraphic architecture reasonably captures the large-scale geometry observed in the field data. However, the finer details evident in the model represent conceptual and interpretative elements introduced to illustrate possible internal layering and channel-edge variability within the Utsira reservoir. These features are not directly resolvable in the seismic data because of its limited vertical and lateral resolution, bandwidth limitations, and signal-to-noise constraints. Consequently, while the model provides valuable insight into plausible depositional and stratigraphic configurations, the correspondence between model and seismic should be viewed as qualitative rather than a one-to-one match of detailed reflectors.

To model the CO_2 effect, brine-to-CO_2 substitution was implemented using a static elastic modeling approach. This method focuses on reproducing the seismic response to fluid replacement without explicitly modeling the time-dependent migration of CO_2. The substitution process assumes that CO_2 occupies a defined portion of the pore space within the reservoir according to the interpreted saturation distribution. These distributions were derived from observed plume geometries in monitor

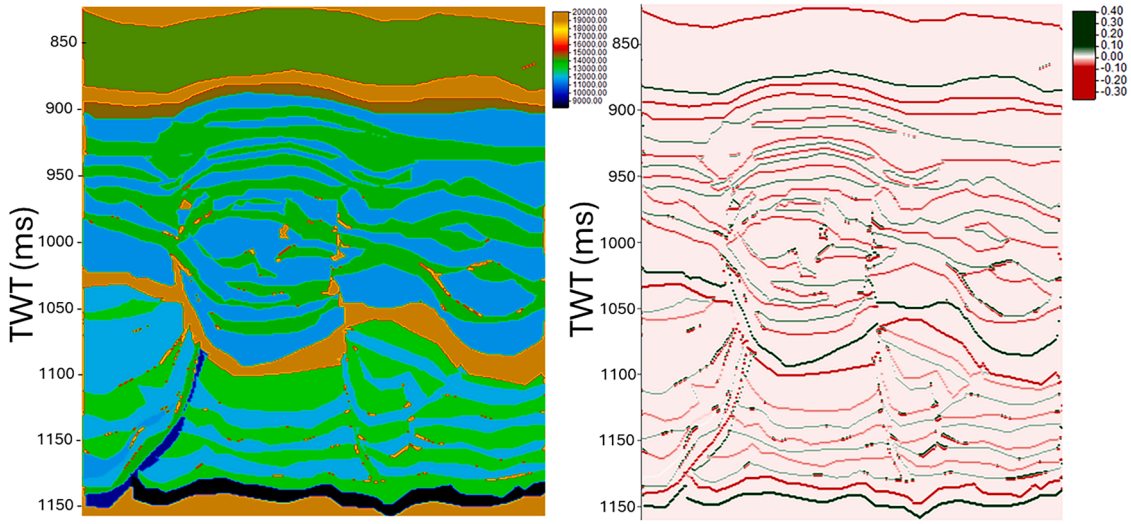

Fig. 4. Acoustic impedance (left) and Reflectivity (right) models used for computing the pre-injection seismic models. The impedance model was computed from assigned rock properties based on well log data and regional geology. The reflectivity model was calculated from the impedance model using Zoeppritz equation. Vertical scale is 1:5.

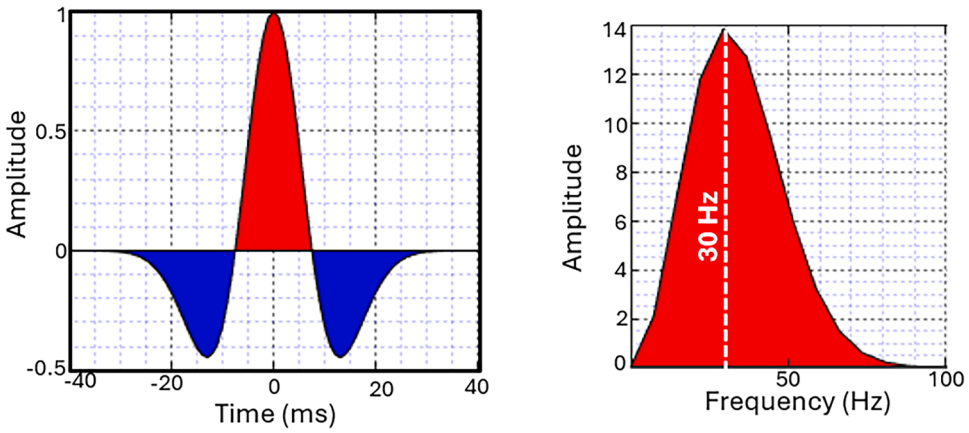

Fig. 5. 30 Hz Ricker wavelet estimated based on the dominant frequency estimated from the actual field seismic data. (Left) Rick wavelet, (Right) amplitude spectrum of the wavelet.

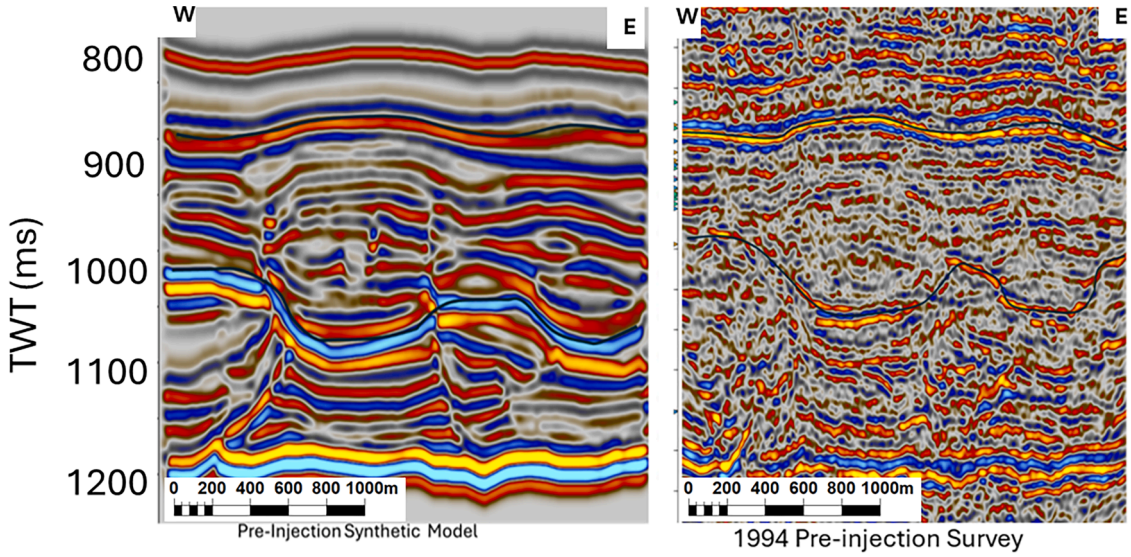

Fig. 6. Compares the synthetic section (left) to the observed 1994 (right) section at X-line 1039 (X-line 1039 is an east-west-oriented seismic crossline located approximately 938 m south of the Sleipner injection point). Visually, the overall patterns of the synthetic model and seismic data appear broadly similar in the absence of noise. The additional details in the model are conceptual and interpretative since the observed seismic resolution is poor. Vertical scale is 1:5 and seismic polarity is European.

surveys and the latest published Sleipner plume maps.

The elastic effect of replacing brine with CO_2 was computed using Gassmann's fluid substitution equation, which predicts how the bulk modulus of a saturated rock changes when the pore fluid is altered. In this formulation, the effective bulk modulus of the saturated rock K_{sat} is given by:

$$K_{sat} = K_{dry} + \frac{\left(1 - \frac{K_{dry}}{K_m}\right)^2}{\frac{\phi}{K_f} + \frac{1-\phi}{K_m} + \frac{K^2_{dry}}{K_m}}$$

where K_{dry} is the dry-frame bulk modulus, K_m is the mineral bulk modulus, ϕ is porosity, and K_f is the effective fluid bulk modulus of the brine–CO_2 mixture. The shear modulus G_{sat} is assumed to remain equal to the dry-frame shear modulus, consistent with Gassmann's assumption of fluid incompressibility under shear deformation.

Once gas substitution (replacing brine with CO_2) is implemented in the model, the seismic properties of the rock, specifically the P-wave velocity (Vp), S-wave velocity (Vs) density (ρ), and acoustic impedance (AI), are recalculated to reflect the new elastic behavior of the rock–fluid system. This involves determining the effective properties of the mixed pore fluid. The bulk modulus K_f and density (ρ) of the new fluid are computed using the saturation fractions of brine (S_w) and CO_2 (S_{CO^2}). The effective fluid bulk modulus is obtained from the harmonic (Reuss) average, given by:

$$\frac{1}{K_f} + \frac{S_w}{K_w} + \frac{S_{CO^2}}{K_{CO^2}}$$

while the mixed fluid density is determined by a linear average

$$\rho_f = S_w\rho_w + S_{CO^2}\rho_{CO^2}$$

where K_w, K_{CO^2}, ρ_w and ρ_{CO^2} are the bulk moduli and densities of brine and CO_2, respectively.

The new saturated bulk modulus of the rock K_{sat} is then calculated using Gassmann's equation. After the new elastic moduli were established, the updated seismic velocities are computed. The compressional velocity (Vp) and shear velocity (Vs) were obtained from:

$$Vp = \sqrt{\frac{K_{sat} + \frac{4}{3}G_{sat}}{\rho_{sat}}}$$

$$Vs = \sqrt{\frac{G_{sat}}{\rho_{sat}}}$$

where the saturated bulk density (ρ_{sat}) is calculated from the mineral and fluid densities as:

$$\rho_{sat} = (1-\phi)\rho_m + \phi\rho_f$$

These parameters describe how the rock's stiffness and inertia change as CO_2 replaces the denser brine. In effect, the introduction of CO_2, being less dense and more compressible than brine, reduces both the bulk modulus and density of the saturated rock. This leads to a decrease in acoustic impedance and, consequently, a higher-amplitude negative reflection (bright spot) or polarity reversal in time-lapse seismic data.

The new acoustic impedance $AI = \rho Vp$ for each layer was recalculated using the updated density ρ and P-wave velocity Vp values obtained from the substitution. The impedance contrasts resulting from the brine-to-CO_2 substitution were convolved with a representative seismic wavelet to generate the synthetic seismic response shown in Fig. 7 (middle). This response represents the modeled post-injection seismic signature, which was then directly compared with both the pre-injection (baseline) model and the observed time-lapse seismic data. In general, the comparison reveals that the synthetic post-injection response closely replicates the main amplitude and polarity characteristics observed in the field time-lapse data. The spatial and vertical continuity of reflectors, associated with CO_2 accumulation, are reproduced, although some differences exist due to noise and the limited vertical resolution of the real seismic data, the broad similarity between the modeled and observed responses supports the validity of the substitution approach and suggests that the modeled impedance variations are possible representative of the CO_2-induced seismic effects within the Utsira Formation.

This static substitution approach allows direct assessment of the seismic sensitivity to CO_2 saturation while maintaining consistency with the known plume geometry. Although it does not account for the dynamic processes of multiphase flow or saturation evolution over time, it provides a computationally efficient and geologically constrained method for isolating the seismic effects of fluid replacement and evaluating the detectability of CO_2 within the reservoir.

2.1. Synthetic evaluation for stratigraphic barriers in CO_2 plume development

Whether the CO_2 plume is trapped by channels or faults remains uncertain. Some interpretations suggest structural confinement related to faulting or gentle structural dips, while others favor stratigraphic control associated with channel geometries. Overall, these interpretations remain speculative because they are primarily based on post-injection monitor surveys, whose seismic reflections are strongly influenced by CO_2 saturation effects. The baseline seismic data, discussed earlier for its limited resolution, does not clearly support either interpretation.

Nwafor et al. (2025) applied sparse-layer spectral inversion to enhance seismic resolution and computed the Stratigraphic Continuity Attribute (SCA) on the improved baseline dataset. The results revealed zones of low seismic continuity at the edges of the plume area, suggesting that these discontinuities may act as lateral barriers to plume migration. However, the exact nature of these edges, whether they represent fault zones, channel boundaries, or mud diapirs as proposed by Chadwick et al. (2004), remains uncertain.

To evaluate the channel-edge hypothesis, we modeled channel scenarios as described above and calculated the SCA on the pre-injection synthetic data using the same workflow applied to the field baseline data. While the synthetic model includes channel-edge terminations, it was constructed independently of the observed field SCA patterns. The purpose was not to reproduce the field data but to test whether channel-like geometries, when subjected to comparable seismic resolution and attribute processing, yield SCA responses similar to those observed in the field. The resulting agreement in Fig. 8, therefore, validates the attribute's diagnostic sensitivity to stratigraphic discontinuities rather than reflecting a circular confirmation of the model. This consistency strengthens the interpretation that the low-continuity edges observed in the baseline data likely correspond to channel margins that influence plume confinement.

This strong agreement between the stratigraphic continuity results of synthetic and actual seismic provides compelling support that the conceptual geologic model likely captures the primary stratigraphic controls on CO_2 plume migration. More specifically, it supports the hypothesis that the discontinuities at the edges of the plume are more likely to be structurally and stratigraphically linked to the channel edge terminations.

2.2. Is the 7–9 meter shale breached?

There has been ongoing debate among scholars regarding whether the thin (7–9 m) shale layer separating the sand wedge from the regional Top Utsira Formation has been breached, allowing CO_2 to migrate into the overlying sand wedge (Cavanagh and Haszeldine, 2014; Chadwick et al., 2004; Furre et al., 2017). A key piece of observational evidence is the time-lapse seismic (4D) data, which displays a bright amplitude anomaly extending above the interpreted top of the Utsira Formation indicated by the blue Horizon in Fig. 9. The apparent time pick of the formation on the monitor data, indicated by the red horizon, is about 23

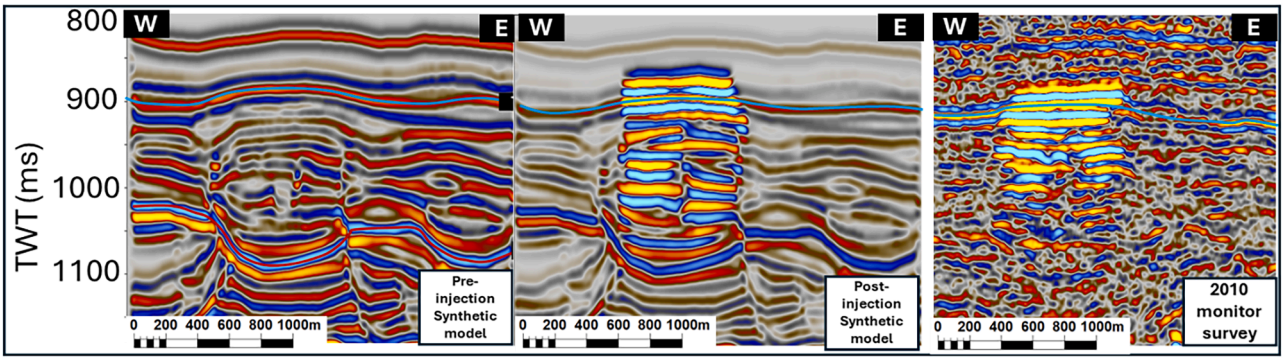

Fig. 7. Comparison of *Synthetic seismic sections for pre- and post-injection scenarios to the 2010 monitor survey*. (a) Brine-saturated case showing baseline synthetic seismic response. (b) Gas-saturated synthetic case illustrating amplitude changes and CO_2 plume-bearing layers, consistent with observed monitor data. c) Actual 2010 monitor data showing plume-induced seismic response. Vertical scale is 1:5 and seismic polarity is European.

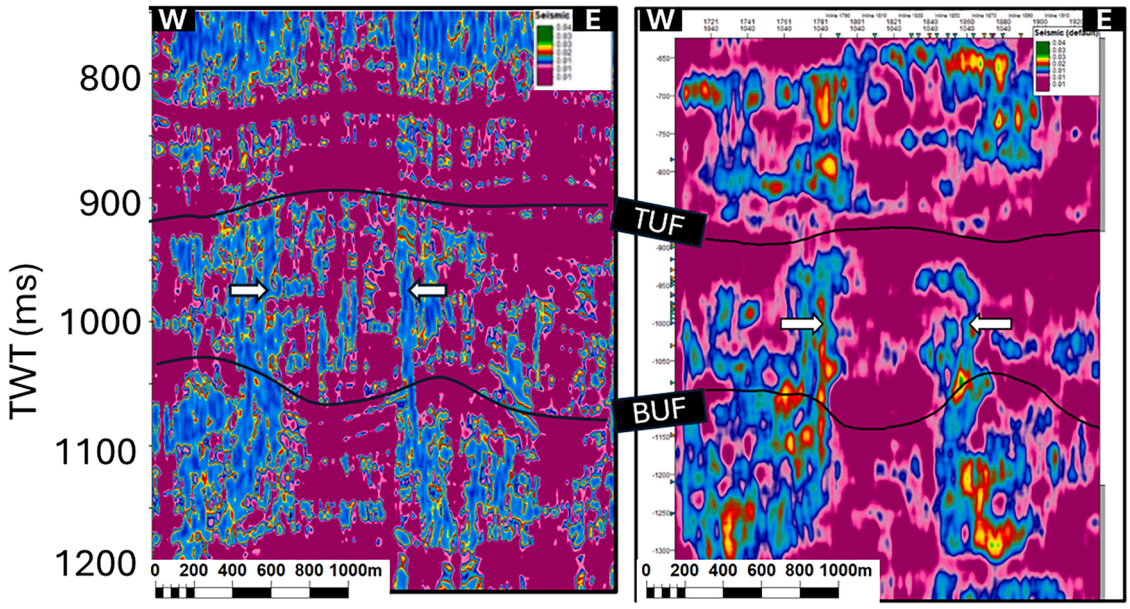

Fig. 8. *Stratigraphic continuity comparison between synthetic and actual pre-injection data.* (a) Synthetic section from the pre-injection model after sparse-layer inversion. (b) Actual pre-injection seismic section at X-line 1040 of the 1994 baseline seismic data. White arrows indicate matching discontinuities at channel edges, supporting the interpretation that plume boundaries are controlled by stratigraphic channel margins. TUF: Top of Utsira Formation, BUF: Base of Utsira Formation. Vertical scale is 1:5.

milliseconds earlier than the pre-injection pick (blue), resulting in apparent "upward shift". Apparent upward shift which is often due to phase shift is when a seismic reflection looks slightly shallower than its true position because the wavelet's phase has changed, not because the actual layer moved. This "upward shift" could provide a clue to resolving this crucial debate.

To explore this, two model scenarios have been proposed to explain CO_2 plume behavior at the top of the reservoir:

1. Scenario 1 (Fig. 10a and b) assumes that the injected CO_2 is trapped beneath the 7–9-meter shale, which acts as an effective internal seal separating the main Utsira sand body from the overlying sand wedge. Illustrated by the conceptual model shown in Fig. 10b
2. Scenario 2 (Fig. 10c and d) assumes that the CO_2 has migrated through or around the thin shale, becoming trapped within the sand wedge above it. Illustrated by the conceptual model shown in Fig. 10d

Notably, Scenario 2 (Fig. 10c and Fig. 10d), in which gas occupies the sand wedge, produced a seismic response more consistent with the actual time-lapse observations. The synthetic data in this scenario reproduced the same apparent upward shift effect at the top of the formation.

It is important to clarify that the observed "upward shift" does not necessarily represent a distinct new anomaly above the reservoir but rather a phase-related elevation shift in the seismic pick, due to a negative 90-degree phase shift of the reflected wavelet in the presence of CO_2. A phase shift in seismic data is a change in the relative phase of the seismic wavelet, resulting in a shift of the apparent position of wavelet peaks, troughs, or zero crossings without changing their frequency. Comparing the gas-filled wedge to the brine-filled wedge, you see a time upward shift and a trough where there was a peak. This is perceived as a -90° phase shift, although the source wavelet is unchanged. The higher impedance contrast from the gas wedge causes stronger reflections and steeper wavelet responses, further enhancing this visual "phase shift."

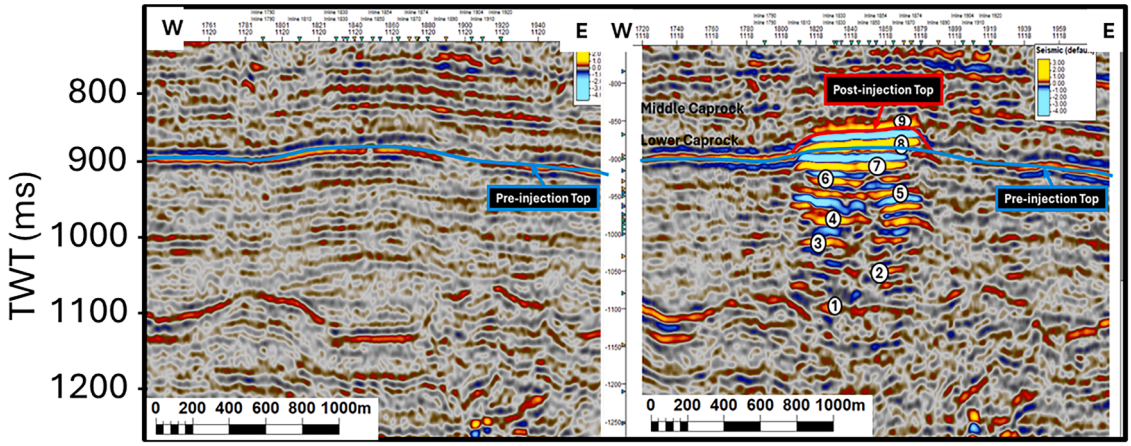

Fig. 9. Seismic sections showing the interpreted Top Utsira Formation. (a) Baseline seismic section (Xline −1120) with the blue horizon marking the pre-injection top pick. (b) 2010 Time-lapse (4D) seismic section (Xline −1118) illustrating an apparent upward shift above the Top Utsira. The red horizon represents the monitor (post-injection) top pick, arriving approximately 23 ms earlier, while the blue horizon shows the pre-injection pick overlaid for comparison. Vertical scale is 1:5 and seismic polarity is European.

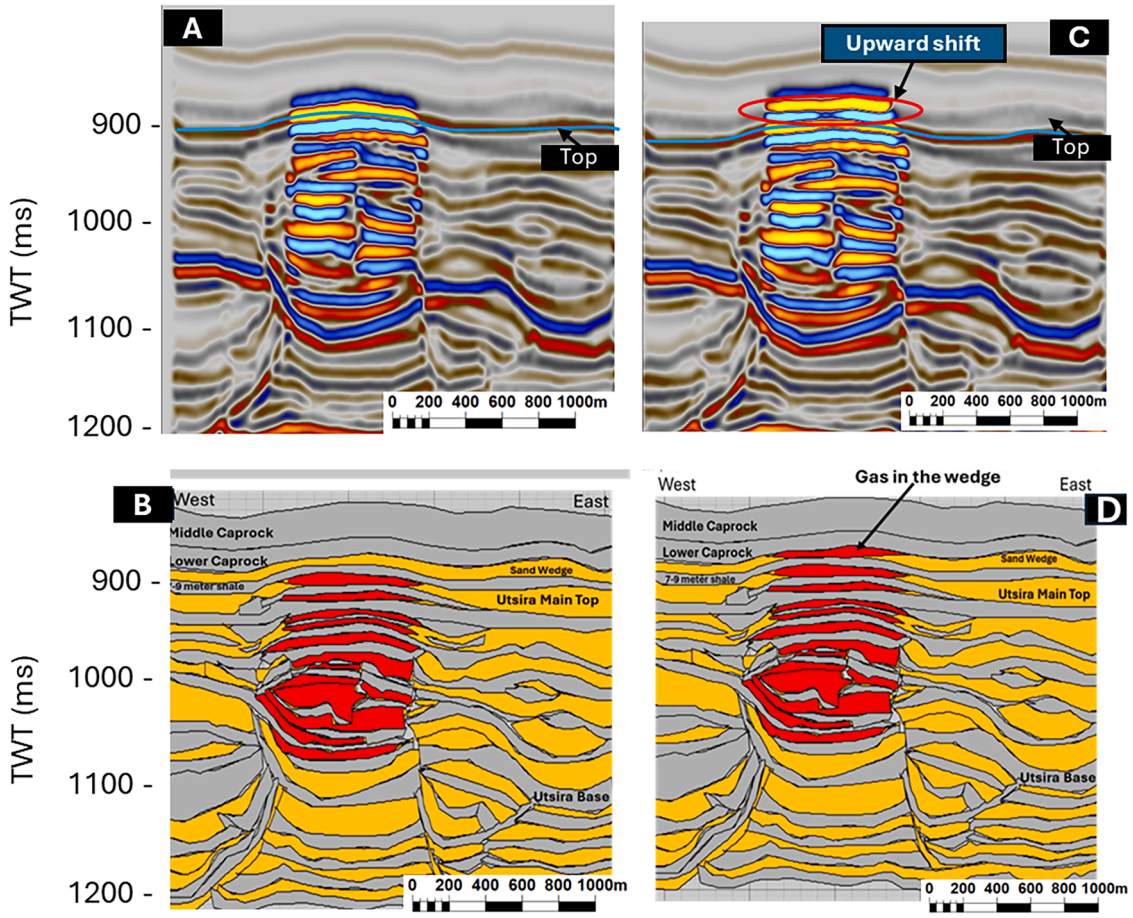

Fig. 10. Conceptual models and synthetic seismic results used to investigate CO_2 plume behavior at the top of the Utsira reservoir. *(a)* Synthetic seismic response for scenarios 1. *(b)* Conceptual model for Scenario 1, where CO_2 is trapped beneath a 7–9 m thick shale layer that acts as an internal seal. *(c)* Synthetic seismic response for Scenario 2, which closely replicates the apparent upward shift effect observed in the time-lapse data, suggesting CO_2 presence in the sand wedge. *(d)* Conceptual model for Scenario 2, where CO_2 has migrated into the overlying sand wedge above the shale layer. Vertical scale is 1:5 and seismic polarity is European.

The fact that this effect is absent in Scenario 1, where no gas is introduced to the sand wedge, and is well-replicated in Scenario 2 may supports the interpretation that the wedge's elastic properties were altered by gas presence, thus mimicking an upward shift and potentially indicating CO_2 migration into the sand wedge.

Comparison between the 2010 monitor seismic response and the synthetic seismic generated for Scenario 2, where CO_2 has migrated into the sand wedge above the internal shale barrier, is illustrated in Fig. 11 below. The field monitor seismic (left) shows a distinct upward shift effect at the top reservoir reflector, interpreted as a result of gas accumulation within the overlying sand wedge. This characteristic seismic signature is closely replicated in the synthetic response (right), suggesting that Scenario 2, CO_2 migration into the sand wedge, provides a more accurate explanation of the observed time-lapse anomaly. The

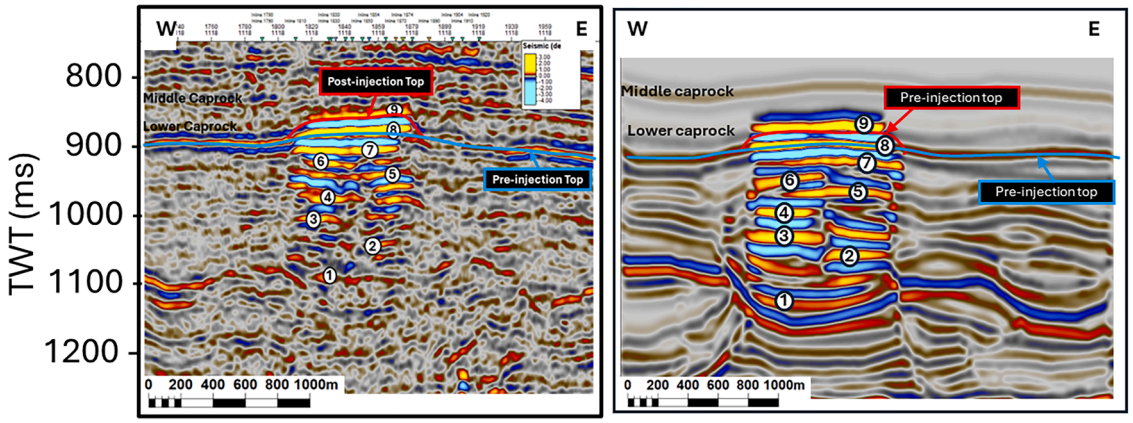

Fig. 11. Comparison of the 2010 monitor seismic with the synthetic response from Scenario 2. The upward shift effect observed in the monitor data is well reproduced by the synthetic model, supporting the interpretation of CO_2 migration into the overlying sand wedge. Vertical scale is 1:5 and seismic polarity is European.

consistency between the observed and modeled data strengthens the interpretation of vertical or lateral CO_2 movement past the thin shale layer.

An alternative explanation for the observed upward phase shift in the time-lapse seismic data can be related to velocity changes associated with CO_2–brine substitution and their treatment during 4D processing. Injection of CO_2 into a saline formation is known to reduce P-wave velocity, which increases travel time through the affected interval. If the migration of the monitor survey is performed using a velocity model derived from the baseline survey, the use of velocities that are locally too high can lead to kinematic mispositioning of seismic events, producing an apparent upward phase or structural shift in the migrated image. Such velocity-model–induced effects are well documented in time-lapse seismic studies and can occur even in the absence of physical breach or bypass of a sealing unit. However, this mechanism typically results in laterally smooth, plume-correlated time shifts that affect reflectors below and within the velocity-perturbed zone in a consistent manner. In contrast, the phase and continuity anomalies observed in this study are spatially confined and stratigraphically focused near the thin shale layer, suggesting that velocity-model effects alone may not fully explain the observed seismic response as demonstrated by the synthetic model.

2.3. Structural vs. stratigraphic control on CO_2 plume trapping

To determine the dominant geologic control on CO_2 plume trapping at the Sleipner field, we compared the structural and stratigraphic capacity margins relative to the plume extent boundaries of the 2010 monitor survey: one based on structural continuity attributes, and the other on stratigraphic continuity attributes. Structural continuity describes the degree to which structural elements—such as faults, folds, fractures, and deformation trends, are laterally and vertically consistent across an area. Stratigraphic continuity on the other hand, refers to the lateral persistence and connectivity of depositional layers, such as beds, facies, and stratigraphic units, through space. The aim was to quantitatively evaluate whether the plume movement is better controlled by topographic structure, lateral structural barriers like fault, or by internal geologic complexity, particularly sand-body connectivity and stratigraphic barriers like channel edges.

2.4. Structural margin capacity relative to plume extent

To assess structural controls on plume migration, several structural attributes were computed from the baseline seismic volume, including dip magnitude, azimuthal gradients, most-negative curvature, passive and aggressive ant-tracking, variance, and fault-likelihood. The most diagnostic attributes, namely; variance, ant-tracking, most-negative curvature, and dip magnitude, were integrated to generate composite structural-continuity maps, which were then compared with the observed plume extent. Fig. 12 (right) illustrates these attributes in an RGB-blended display, allowing simultaneous visualization of structural influence on plume geometry, delineated by the blue overlay polygon. Warm colors correspond to structurally complex zones characterized by high variance, steep dips, strong curvature, and dense, irregular linear features associated with discontinuities emphasized by the ant-tracking attribute. In contrast, cool colors denote relatively homogeneous regions with low variance, gentle dips, and low curvature, indicating fewer discontinuities. The strong spatial correspondence among the attributes demonstrates internal consistency in their structural response. Notably, the plume polygon lies within, though not confined to, these structurally complex zones.

Fig. 12 (left) shows a crossline section of the variance attribute blended with the ant-tracking volume. It is important to note that while the variance attribute highlights waveform discontinuities caused by faults or stratigraphic changes, the ant-tracking algorithm enhances and linearizes these discontinuities to mimic fault-like patterns. Consequently, not all the linear features observed in Fig. 12 necessarily represent true faults. The white arrows highlight probable structural features that may bound the plume area.

The Structural margin capacity $m_{capacity}$ was calculated by delineating the area enclosed by these structural continuity regions, $A_{structure}$, that encompasses the CO_2 plume (area polygons are overlaid on Fig. 10b), A_{plume}. Assuming the plume area, A_{plume}, is fully contained

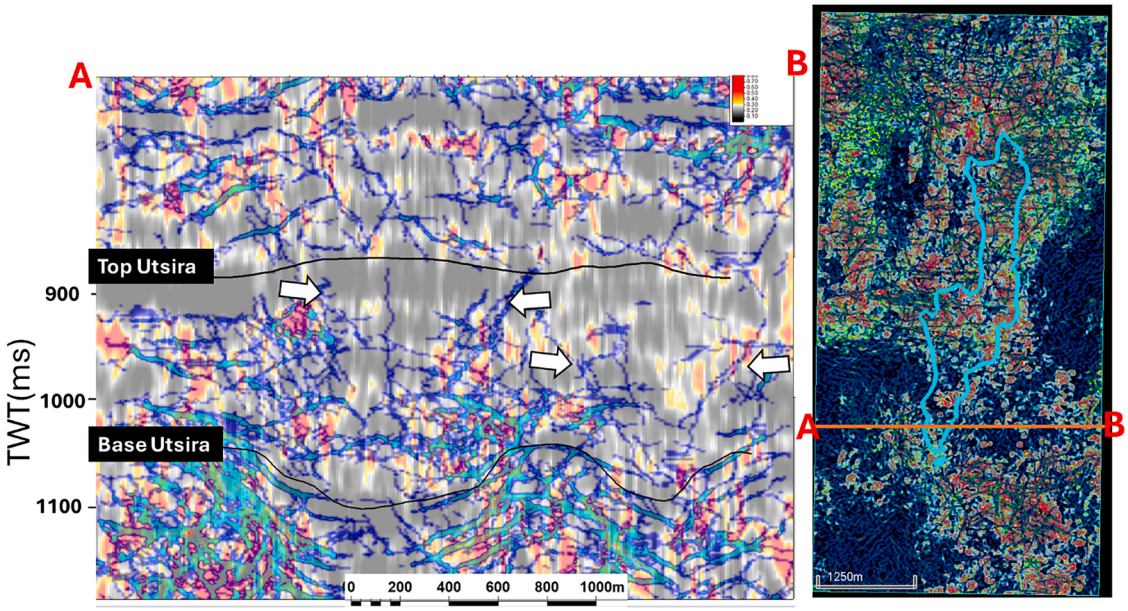

Fig. 12. Structural continuity analysis for evaluating plume–structure relationships on the 1994 baseline survey. (left) Crossline (Xline 1048) section showing variance blended with ant-tracking attributes. Variance highlights waveform discontinuities that may result from faults or stratigraphic changes, while ant-tracking enhances and linearizes these discontinuities to mimic fault-like patterns. Arrows indicate probable structural features bounding the plume area; however, not all linear features necessarily represent true faults. (right) RGB-blended time slice (at 912 milliseconds) integrating variance, ant-tracking, most-negative curvature, and dip-magnitude attributes, with the plume geometry outlined by the blue polygon. Warm colors represent structurally complex zones characterized by high variance, steep dips, and strong curvature, whereas cool colors correspond to relatively homogeneous regions with fewer discontinuities. Vertical scale is 1:5.

within this structural complex zone, the Structural margin capacity is defined as:

$$m_{\text{capacity}} = 1 - f_{\text{cover}} = \left(\frac{A_{\text{structure}} - A_{\text{plume}}}{A_{\text{structure}}}\right)$$

Where f_{cover} is the coverage ratio. The coverage ratio is defined as the ratio of the plume area A_{plume} to the total structural area, $A_{\text{structure}}$. This parameter measures the fraction of the structural domain occupied by the plume. A high f_{cover} (approaching 1) indicates that the plume nearly fills the structural closure and could be structurally trapped, while a low value suggests that most of the structural capacity remains unused. The capacity margin (m_{capacity})quantifies the remaining unoccupied portion of the structure. The analysis result shown in Table 2 indicates that plume occupies only 15 % of the structural area, and 85 % of the potential structural capacity remains unused, suggesting that the plume is not structurally trapped; it is still spreading within the broader structural domain rather than filling or being confined by it.

2.5. Stratigraphic margin capacity relative to plume extent

To assess the stratigraphic control, the SCA map was calculated from the baseline 3D seismic data to highlight the stratigraphic boundaries (channel edges) as shown in Fig. 13 below. The white arrows in 13 (left) point to the stratigraphic boundaries on the crossline section, and 13 (right) is the map showing the channel geometry with the plume extent (light blue polygon) overlay. The Stratigraphic margin capacity m_{capacity} was calculated by delineating the area enclosed by the stratigraphic boundaries, $A_{\text{stratigraphic}}$, that encompasses the CO_2 plume area, A_{plume}. Assuming the plume area, A_{plume}, is fully contained within this stratigraphic continuity zone, the Stratigraphic margin capacity is defined as:

$$m_{\text{capacity}} = 1 - f_{\text{cover}} = \left(\frac{A_{\text{stratigraphy}} - A_{\text{plume}}}{A_{\text{stratigraphy}}}\right)$$

Where f_{cover}, the coverage ratio is defined as the ratio of the plume area A_{plume} to the total continuity area within the stratigraphic boundaries, $A_{\text{stratigraphy}}$.

This parameter measures the fraction of the stratigraphic domain occupied by the plume. A high f_{cover} (approaching 1) indicates that the plume nearly fills the area within the stratigraphic boundary and could be stratigraphically trapped, while a low value suggests that most of the stratigraphic capacity remains unused. The margin capacity (m_{capacity})quantifies the remaining unoccupied portion of the SCA area. Table 3 indicates that the plume fills about 82 % of the compartmentalized stratigraphic area, and only 18 % remains unoccupied; it is approaching but not fully constrained by the compartment. The remaining capacity indicates partial influence of stratigraphic boundaries but no filled yet. A later monitor survey acquired in 2020 shows that the plume has expanded further, possibly filling up the remaining 18 % and is beginning to migrate westward.

A closer examination of the structural attribute section in Fig. 14, generated by blending the variance and ant-tracking attributes, reveals that the injection area is bounded by distinct "V"-shaped edges (outlined by red dashed lines) at both point A (the injection location) and point B to the east. Within these V-shaped margins, the attribute values indicate low variance (high coherence), suggesting high stratigraphic continuity. The linear features highlighted by white arrows and red dashed outlines in the interpreted section (right) are more plausibly interpreted as incision or channel edges rather than faults, as there is no observable vertical offset at the top of the Utsira Formation to suggest fault displacement. Additionally, subhorizontal reflectors, delineated by orange dashed lines, terminate against these edges, typical of incised or channelized strata. The feature marked 'B' is likely another incision to the east. The near-vertical feature marked by the red arrow is interpreted as a possible migration conduit, consistent with previously discussed pathways for vertical CO_2 movement.

The overlay of the blended structural attribute on the 2010 monitor survey in Fig. 15 shows the plume imprint aligning precisely fitting into the incised valley (or channel) system. This strong spatial correspondence indicates that plume migration was mostly guided by the pre-existing stratigraphic architecture rather than by structural trapping, suggesting that the plume followed the pathway of the incised channel and was likely stratigraphically confined as established above. The red arrow marks a vertical migration conduit that cuts through the intra-channel layers, illustrating how the plume likely migrated upward through the thin internal drape shales identified in the well logs and documented regionally in previous studies.

Table 2
Quantitative parameters showing the relationship between plume and structural areas.

Parameters	Symbol	Formular	Value (m^2)	Interpretation
Plume Area	A_{plume}	-	2170,657.6	-
Structure Area	$A_{\text{structure}}$	-	14,396,715	-
Coverage ratio	f_{cover}	$A_{\text{plume}}/A_{\text{structure}}$	0.1508 (≈ 15.1 %)	Plume occupies only ~15 % of the structural capacity
Capacity Margin	m_{capacity}	$1 - f_{\text{cover}}$	0.8492 (≈ 84.9 %)	About 85 % of the structure remains unfilled

3. Conclusions

The results of this study demonstrate that internal stratigraphic architecture exerts the dominant control on CO_2 plume migration and trapping within the Utsira Formation, rather than structural confinement. Quantitative analyses using the newly developed plume coverage ratio and margin capacity metrics reveal that only about 18 % of the mapped stratigraphic boundary remains unfilled, whereas approximately 85 % of the potential structural capacity is unutilized. This contrast clearly indicates that plume confinement is primarily governed by stratigraphic features such as channel-edge terminations and intra-formational shale drapes, which compartmentalize flow within the reservoir and act as effective lateral baffles to CO_2 migration.

The structural capacity evaluation further supports this interpretation, showing that the plume occupies only around 15 % of the total structural domain. This low occupancy implies that the CO_2 plume is not trapped within a structural closure but continues to spread laterally within the broader depositional framework. The alignment between the plume extent and low-continuity channel margins observed in the stratigraphic continuity attribute (SCA) maps further confirms that lateral migration pathways are largely defined by depositional geometry and stratigraphic heterogeneity rather than fault-bounded structures.

Synthetic seismic modeling results also provide strong evidence of localized shale bypass or partial breach of the 7–9 m internal shale barrier that separates the main Utsira reservoir from the overlying sand wedge. Among the two conceptual scenarios tested, the model allowing upward CO_2 migration through or around this thin shale layer successfully reproduced the observed "upward shift" anomaly in the time-lapse seismic data. This correspondence suggests that the shale barrier may not be fully sealing but instead allows limited gas migration into the overlying sand wedge.

The close agreement between the synthetic and field seismic responses validates the conceptual model and confirms that the applied static elastic substitution approach mostly captures the key acoustic and elastic effects associated with CO_2 saturation changes. The modeled impedance variations successfully reproduced the amplitude responses, and reflector continuity patterns observed in the monitor surveys, supporting the model assumptions and workflow.

The results also highlight that CO_2-induced velocity changes can

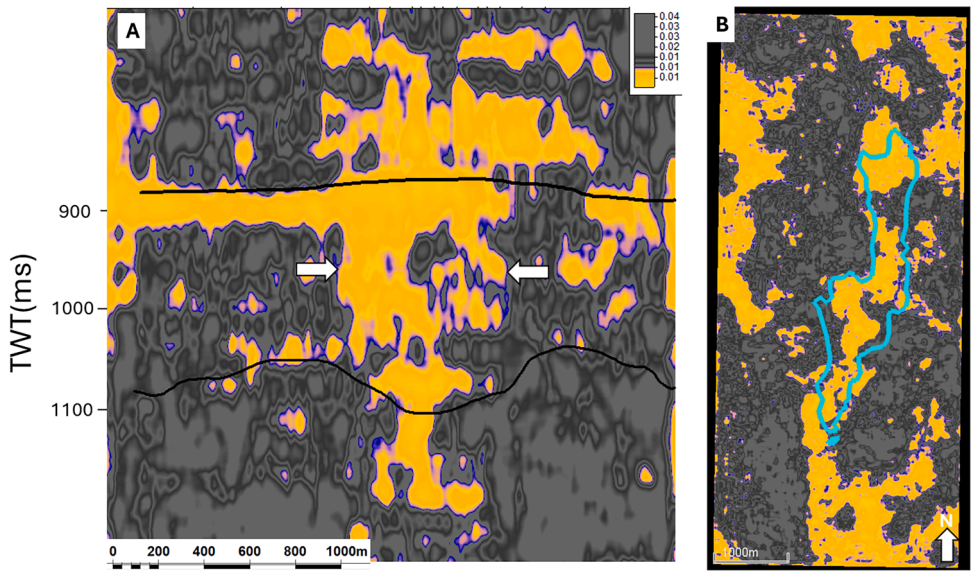

Fig. 13. Stratigraphic Continuity Attribute (SCA) analysis on the 1994 baseline survey showing channel geometry and plume extent. (left) Crossline (Xline 1048) view highlighting stratigraphic boundaries (white arrows). (right) SCA time-slice at 950 milliseconds displaying channel margins with the CO_2 plume (light-blue polygon) overlay. The stratigraphic margin capacity compares the area enclosed by stratigraphic boundaries to the plume area. Vertical scale is 1:5.

Table 3
Quantitative parameters showing the relationship between plume and stratigraphic areas.

Parameters	Symbol	Formular	Value (m^2)	Interpretation
Plume Area	A_{plume}	-	2170,657.6	-
Structure Area	$A_{stratigraphy}$	-	2649,415.6	-
Coverage ratio	f_{cover}	$A_{plume}/A_{stratigraphy}$	0.8193 ≈ 81.9 %	Plume occupies ~82 % of the stratigraphic capacity
Capacity Margin	$m_{capacity}$	$1 - f_{cover}$	0.1807 ≈ 18.1 %	Only ~18 % of the stratigraphic area remains unfilled

significantly alter the apparent structural geometry of underlying reflectors in seismic data. These velocity reductions, resulting from brine-to-CO_2 substitution, may produce time-shift effects that mimic structural deformation, potentially complicating the separation of stratigraphic and structural influences on plume trapping. While this study focused on distinguishing the relative roles of internal stratigraphy and structure, a quantitative assessment of the magnitude and spatial extent of velocity-induced distortions is reserved for future work. Such analysis will be crucial for refining seismic interpretation and improving the accuracy of plume geometry reconstruction in CO_2 storage monitoring.

We conclude that CO_2 plume evolution at the Sleipner site is primarily governed by stratigraphic compartmentalization within the Utsira Formation. Internal heterogeneities such as thin shale drapes, channel terminations, and incised-valley geometries strongly influence plume shape, lateral spread, and vertical migration is controlled by intraformational polygonal faults. These findings emphasize the importance of high-resolution stratigraphic characterization and seismic attribute analysis for improving predictive models of plume migration and for guiding the monitoring and risk assessment of future geological carbon storage projects.

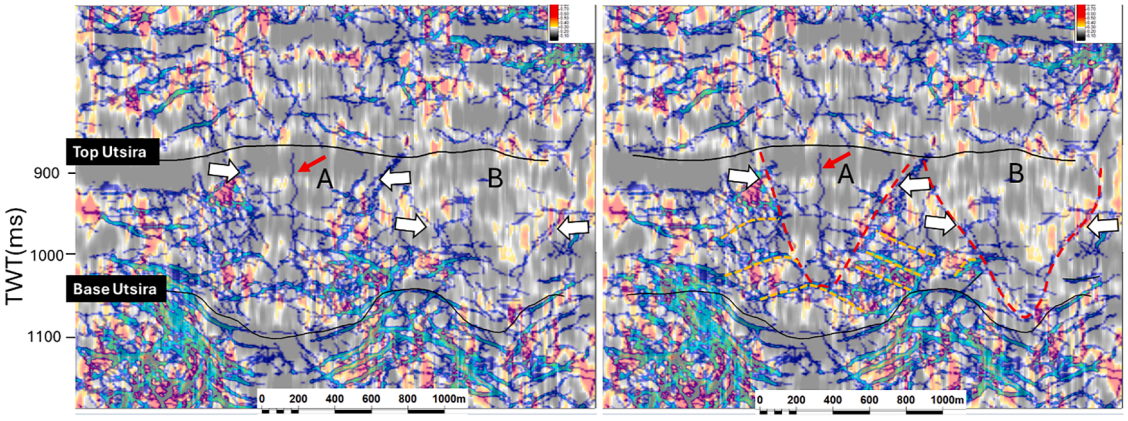

Fig. 14. Structural attribute section showing the relationship between structural and stratigraphic features around the injection area on the baseline survey. (left) Uninterpreted variance–ant-tracking blended section highlighting "V"-shaped edges near the injection site. (right) Interpreted view showing these edges (red dashed lines) at points A and B, interpreted as incision or channel margins rather than faults due to the absence of vertical offset at the top of the Utsira Formation. Low-variance (high-coherence) zones within the V indicate high stratigraphic continuity, while horizontal reflectors (orange dashed lines) terminate against the channel edges, typical of incised stratigraphy. The vertical feature marked by the red arrow likely represents the polygonal fault serving as a migration conduit for upward CO_2 movement. Vertical scale is 1:5.

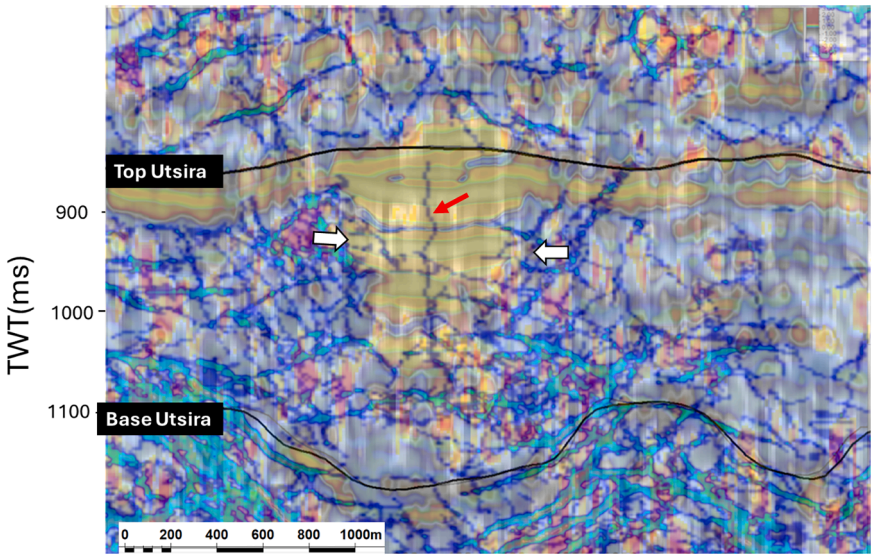

Fig. 15. Overlay of the baseline blended structural attribute on the RMS amplitude of section 2010 monitor survey showing the CO_2 plume imprint confined within the incised valley (or channel). The close fitting between the plume and the channel geometry indicates more of stratigraphic rather than structural lateral control on plume migration. The red arrow marks the polygonal fault, a vertical conduit cutting through intra-channel sediments, illustrating upward migration through thin internal drape shales observed in well logs and reported by previous studies. Vertical scale is 1:5.

CRediT authorship contribution statement

Basil Onyekayahweh Nwafor: Writing – original draft, Project administration, Methodology, Investigation, Formal analysis, Data curation, Conceptualization. **John P. Castagna:** Supervision, Methodology. **Robert Van Eykenhof:** Validation, Formal analysis. **Marianne Rauch:** Writing – review & editing, Validation, Software. **David E. Bass:** Writing – review & editing, Data curation.

Declaration of competing interest

The authors declare that they have no known competing financial interests or personal relationships that could have appeared to influence the work reported in this paper.

Data availability

Data will be made available on request.

References

Arts, R., Eiken, O., Chadwick, A., Zweigel, P., van der Meer, L., Zinszner, B., 2004. Monitoring of CO_2 injected at Sleipner using time-lapse seismic data. Energy 29 (9–10), 1383–1392. https://doi.org/10.1016/j.energy.2004.03.072.

Arts, R., Eiken, O., Chadwick, A., Zweigel, P., van der Meer, L., Zinszner, B., 2008. Monitoring CO_2 storage at Sleipner using time-lapse seismic data. Energy 33 (2), 209–217. https://doi.org/10.1016/j.energy.2004.03.072.

Benson, S.M., Cole, D.R., 2008. CO_2 sequestration in deep sedimentary formations. Elements 4 (5), 325–331. https://doi.org/10.2113/gselements.4.5.325.

Cavanagh, A.J., Haszeldine, R.S., 2014. The Sleipner storage site: capillary flow modeling of a layered CO_2 plume requires fractured shale barriers within the Utsira Formation. Int. J. Greenh. Gas Control 21, 101–112. https://doi.org/10.1016/j.ijggc.2013.12.018.

Chadwick, A., Arts, R., Eiken, O., Zweigel, P., & van der Meer, B. (2004). 4D seismic quantification of a growing CO_2 plume at Sleipner, North Sea. In Proceedings of the 7th International Conference on Greenhouse Gas Control Technologies (pp. 1383–1388). https://api.semanticscholar.org/CorpusID:128997616.

Chadwick, R.A., Noya, D., Arts, R., Eiken, O., 2009. Latest time-lapse seismic data from Sleipner yield new insights into CO2 plume development. Energy Procedia 1, 2103–2110. https://doi.org/10.1016/j.egypro.2009.01.274.

Chadwick, A., Williams, G., Delepine, N., Clochard, V., Labat, K., Sturton, S., Arts, R., 2010. Quantitative analysis of time-lapse seismic monitoring data at the Sleipner CO_2 storage operation. Lead. Edge 29 (2), 170–177. https://doi.org/10.1190/1.3304820.

Furre, A.-K., Warchoł, M.J., Alnes, H., Pontén, A.S.M., 2024. Sleipner 26 years: how well-established subsurface monitoring work processes have contributed to successful offshore CO2 injection. Geoenergy Sci. Technol. 2, 1–15. https://doi.org/10.1144/geoenergy2024-015.

Furre, A.K., Eiken, O., Alnes, H., Vevatne, J.N., Kiær, A.F., 2017. 20 years of monitoring CO_2-injection at Sleipner. Energy Procedia 114, 3916–3926. https://doi.org/10.1016/j.egypro.2017.03.1523.

IPCC, 2005. Special Report on Carbon Dioxide Capture and Storage. Intergovernmental Panel On Climate Change. Cambridge University Press.

Nwafor, B.O., Castagna, J., Stewart, R., 2024. Deciphering CO2 reservoir dynamics: geophysical analysis of carbon capture and storage at Sleipner Field. In: International Meeting for Applied Geoscience & Energy (IMAGE), 2024. Offshore, North Sea, p. 1.

Nwafor, B.O., Robert, V.E., John, P.C., Marianne, R., 2025. A deeper understanding of Sleipner's CO2 pre-injection geology through the stratigraphic continuity attribute. 86th EAGE Annual Conference & Exhibition, Toulouse France, 2025. https://doi.org/10.3997/2214-4609.2025101229.

Rauch, M., Nwafor, B.O., Eykenhof, V.R., Castagna, J., 2025. Under the Surface of Sleipner: What Sparse Layer Inversion Reveals About CO_2 Storage. European Association of Geoscientists & Engineers 2025, 1–5. https://doi.org/10.3997/2214-4609.202585012.

Warchoł, M.J., Pontén, A., Furre, A.-K., 2025. Stratigraphic controls on CO2 migration at Sleipner: an example from a basin-floor fan of the Utsira Formation. Basin Res. 37, e70018. https://doi.org/10.1111/bre.70018.

Williams, G.A., Chadwick, R.A., 2021. Influence of reservoir-scale heterogeneities on the growth, evolution, and migration of a CO2 plume at the Sleipner Field, Norwegian North Sea. Int. J. Greenh. Gas Control 106. https://doi.org/10.1016/j.ijggc.2021.103260.

Zweigel, P., Arts, R., Lothe, A.E., Lindeberg, E., 2004. Geological Storage for CO2 Emissions Reduction. In: Baines, S., Gale, J., Worden, R.H. (Eds.), vol. 233. Special Publication of the Geological Society, London, pp. 165–180.